Payri, R.; Marti-Aldaravi, P.; Montiel-Prieto, T.; Viera, A. (2020). Influence of aging of a diesel injector on multiple injection strategies. Applied Thermal Engineering. 181:1-9. https://doi.org/10.1016/j.applthermaleng.2020.115891

Published as: Applied Thermal Engineering, vol. 181, no. August, p. 115891, 2020. DOI: 10.1016/j.applthermaleng.2020.115891.

Influence of aging of a diesel injector on multiple injection strategies

Raul Payri[a,*], Pedro Martí-Aldaraví[a], Tomas Montiel[a], Alberto Viera[b]

[a] *CMT - Motores Térmicos, Universitat Politècnica de València, Edificio 6D, 46022, Valencia, Spain.*
[b] *AVL Iberica SA, Edificio El Rengle Nucleo D, 08302, Mataro, Barcelona.*

Abstract

Multiple injection strategies have contributed to the improvement of thermal processes in Internal Combustion Engines. On this matter, the correct performance of the injector is a critical factor in the implementation of these techniques, as changes in the behavior of the injector could affect the injection development, altering the combustion process and heat transformation efficiency. Thus, the present study analyzes the development of multiple injection events in a diesel injector aged due to partial obstruction of the holes of the nozzle. To this end, a multi-hole piezoelectric injector was employed, in which the aging of the injector is evaluated through momentum flux measurements for each hole. Afterwards, rate of injection tests with pilot and post injection strategies are performed, and the results are compared to the injection events made by the same injector before aging. The results provided by the momentum flux experiments confirmed the partial obstruction of two holes. Furthermore, rate of injection comparisons showed that the injector had a lower steady-state rate of injection after aging and required a longer time to end the injection. These phenomena affected the multiple injection events, as the extended time required to end the injection reduced the hydraulic dwell time between pilot/post injection and the main injection. Furthermore, for short dwell times, this phenomenon led to the unification of the main and post injection, resulting in a large single

*Corresponding author. E-mail address: rpayri@mot.upv.es

Published as: Applied Thermal Engineering, vol. 181, no. August, p. 115891, 2020. DOI: 10.1016/j.applthermaleng.2020.115891.

injection. Hence, not only an increase in fuel consumption would appear, but the thermal benefits of implementing the post injection would be lost.

Keywords: Aging, diesel injection, rate of injection, multiple injections

1. Introduction

Due to strict environmental and fuel economy standards set in recent legislations [1], researchers have been motivated to find a continuous development of multiple areas of the internal combustion engine. Regarding the diesel injection process, multiple injection strategies are one of the numerous techniques implemented in modern diesel engines to reduce its emissions [2]. Among multiple injection techniques, pilot injections have been found to reduce combustion noise and nitrogen oxides (NO_x) emissions [2–4]. In general terms, pilot injections decrease the ignition delay of the main pulse, by enhancing conditions for its combustion. As a result, the amount of fuel burned in the premixed phase is reduced, which leads to a reduction in the combustion peak temperature [2], determinant for the formation of NO_x [5, 6]. Regarding post injection strategies, literature work widely refers to this technique as a tool for the reduction of soot exhaust emissions [7, 8]. Specifically, a post injection introduces momentum in the latter phase of combustion, which also enhances mixing within the cylinder bowl and the oxidation of soot formed by the main injection [9, 10].

Nevertheless, to fully achieve the mentioned improvements from multiple injection techniques, the proper hydraulic response of the injector is crucial, as these techniques largely rely on the correct injection timing and temporal space between injections (dwell time), as well as the amount of fuel injected. Zheng et al. [11] studied the influence of the pulses intervals on combustion and emissions of blended fuels under high EGR (46%), finding that increasing the pilot-main interval resulted in a reduction of the smoke emissions but increased the carbon monoxide (CO) and total hydrocarbons (HC) emissions, whereas NO_x emissions first decreased and then increased with increasing dwell times.

On the other hand, they found that increasing the main-post interval reduced the peak of post heat release rate and NO_x emissions whereas CO and total HC emissions deteriorated, and smoke emissions first increased and then declined with increasing dwell times. Furthermore, Yoon et al. [12] analyzed the diesel particulate filter regeneration with a post injection at low and medium load. They found relevant to tune both the timing and number of pulses to achieve proper exhaust temperatures with an acceptable compromise in terms of unburned HC and CO emissions. Moreover, Liu et al. [13] investigated the optimal pilot injection strategy under gasoline compression ignition in a diesel engine and found that the use of optimized pilot injection, in terms of dwell time and mass injected, constantly achieved lower pressure rise rate and soot emissions than the single injection baseline.

The mentioned studies serve to depict the importance of having precise injection timings in multiple injection strategies. Consequently, variations of the hydraulic performance of an injector have become a matter of interest, including alterations due to the aging of the injector [14]. In particular, several authors have underlined variations in the injection process due to the presence of deposits in the outlet orifices, which could appear due to the nozzle geometry, fuel composition, high temperatures or manufacturing defects [15]. Winterbone et al. [16] reported a non-uniform spray distribution and lower steady rate of injection ($\dot{m}$), due to a reduction in the flow area of the nozzle as the fouling appeared. Moreover, Richards et al. [17] found a shortening of the lift-off length and spray penetration, because of the additional heat transferred from the deposits to the outlet fuel. This phenomenon resulted in shorter ignition delays and low-quality mixing processes, increasing exhaust emissions.

Moreover, Hofmann et al. [14] analyzed the influence of worn nozzles in the injection rate. To this end, three injectors with different outlet orifices diameter were employed: the worn nozzle was compared to a nozzle with larger outlet orifices (simulating cavitation effects), and to a nozzle with smaller orifices (emulating deposits presence) and the results showed that the worn nozzle had similar maximum injection rate than the injector with smaller orifices. The authors

attributed this phenomenon to nozzle constriction due to fouling. Additionally, deposits can appear inside the body of the injector [18] as well, which could restrict the hydraulic flow and affect the engine power and fuel consumption [19]. Furthermore, fouling near the injector needle has been observed, producing a needle sticking phenomenon which would result in slower hydraulic responses to the electric pulse sent to the injector [20], or preventing the injector from opening at low injection pressures [21].

Therefore, aging of the diesel injector due to the presence of deposits could deteriorate its hydraulic behavior, affecting the multiple injection strategies. On this matter, previous works related to aging mainly focused on its effects on a single injection. Additionally, many of the mentioned investigations have employed an already fouled injector and compared it with other injectors with different nozzle geometry. In contrast, this work focuses on the performance of the same multi-hole diesel injector before and after aging, comparing the rate of injection (ROI) at the beginning of its lifetime, to the injection rate provided by the injector after aging. Thus, differences in the hydraulic response of the same injector before and after aging were analyzed. Additionally, the experiments were done employing multiple injection pulses, focusing on the aging effects on pilot and post injection strategies. In the following sections, the equipment used within the measurements is described. Then, the results obtained are detailed and discussed. Finally, the main conclusions of the work are drawn.

2. Materials and methods

In the current section, a description of the equipment and methods used throughout the experiments is done. These measurements were made at two stages of the lifetime of the injector: once when it was brand new, and another after 1400 hours of use, with an injection frequency of 0.25 Hz. Furthermore, all of the injection cycles made with the injector throughout its lifetime were done employing commercially available diesel fuel (EN590), and inside the CMT facilities. Thus, the aging process and injection boundary conditions the injector

Published as: Applied Thermal Engineering, vol. 181, no. August, p. 115891, 2020. DOI: 10.1016/j.applthermaleng.2020.115891.

Nomenclature

A_{eff}	Effective area	IRDCI	Injection rate discharge curve indicator
A_o	Theoretical outlet area		
BP	Back Pressure	$\dot{M}$	Steady momentum flux
CO	Carbon monoxide	$\dot{m}$	Steady rate of injection
C_M	Momentum flux coefficient	NO_x	Nitrogen oxides
C_a	Area coefficient	ρ_f	Density of the fuel
C_d	Discharge coefficient	ΔP	$P_{inj} - P_{back}$
HC	Hydrocarbons	P_{back}	Back pressure
DT	Dwell time	P_{inj}	Injection pressure
EOE	End of energizing	ROI	Rate of injection
EOI	End of injection	SOE	Start of energizing
ET	Energizing time	SOI	Start of injection
HD	Hydraulic delay		

went through are known. Specifically, the injector was employed in a high pressure and high temperature test rig. Within this test rig, the combustion chamber operated at temperatures ranging from 800 K to 1100 K and pressures up to 20 MPa, simulating real engine conditions. This test is rig thoughtfully detailed by Payri et al. [22].

2.1. Fuel delivery system

Initially, fuel is retrieved from a tank and sent through a purger to separate the air, followed by a filter to remove particles and impurities contained in the fuel. Then, the required combustible goes inside a CP3 pump, where its pressure is raised to the desired injection pressure and then sent to the common-rail, where it is contained. Thus, a relatively large volume of diesel at high pressure is available to deliver whenever it is requested. On the other hand, the excess of fuel coming out of the pump is sent back to the purger along with the excess fuel returning from the common rail. Before getting to the purger, the diesel fuel is directed through a heat exchanger, where its temperature is controlled.

Published as: Applied Thermal Engineering, vol. 181, no. August, p. 115891, 2020. DOI: 10.1016/j.applthermaleng.2020.115891.

The injector used throughout the experiments was the latest iteration of the commercially available piezo common-rail (PCR) type 5 from Continental [23]. It has six holes in the nozzle and can manage up to 250 MPa of injection pressure. The main characteristics of the injector, at its new state, are presented in Table 1. A nozzle with high k-factor [24] was selected given that increasing the conicity, significantly suppresses cavitation appearance inside the nozzle orifices [25, 26]. The geometry of the injector was provided by the manufacturer.

Table 1: Nozzle geometry.

Parameter	**Value**	**Units**
Number of holes	6	-
Avg. holes diameter ($\overline{D}_o$)	90.1	μm
Avg. height angle	75	$degrees$
Avg. k-factor	5.3	-
Nominal flow rate	313*	$mL\,min^{-1}$
Degree of hydro-erosion	7.7	%

* At 10 MPa of injection pressure.

2.2. Test rigs

2.2.1. Momentum Flux Test Rig

Momentum flux measurements were done to assess the status of the outlet orifices of the injector, as this technique allowed the study of each hole of the nozzle individually. In Figure 1, part of the equipment used is shown. High pressure fuel is delivered to the injector, which is located on top of the test rig chamber, immersed in circulating coolant (ethylene glycol at 30 % pumped at a rate of 60 L/min), in order to take its temperature up to 363 K. This proceeding is essential, as the performance of a piezoelectric injector greatly depends on its working temperature [27]. Furthermore, the nozzle of the injector reaches the chamber, in which the spray of interest is faced with a pressure sensor. This pressure sensor is mounted on the sensor holder and employed to measure the impact force of the spray during the injection.

Published as: Applied Thermal Engineering, vol. 181, no. August, p. 115891, 2020. DOI: 10.1016/j.applthermaleng.2020.115891.

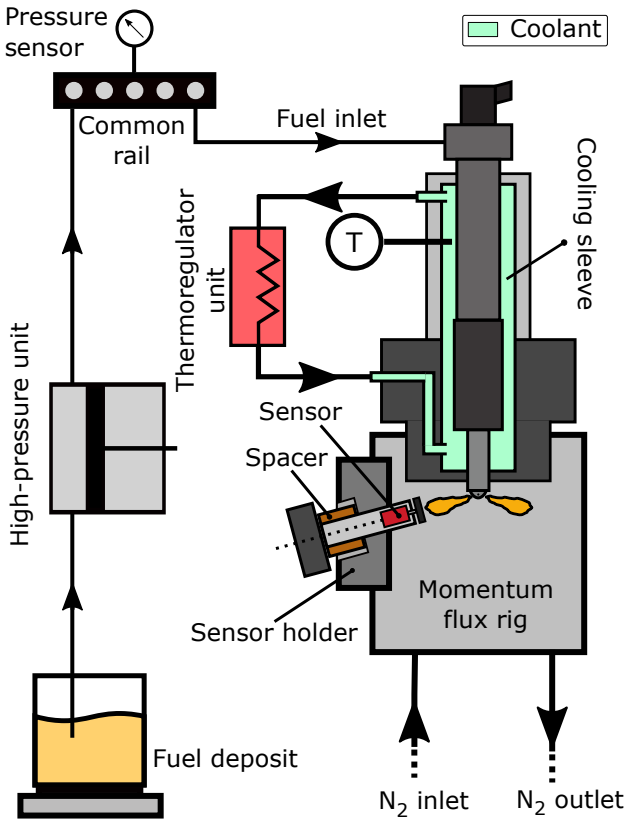

Figure 1: Momentum flux test rig schematic diagram.

Additionally, spacers are used to separate the sensor from the nozzle tip at a convenient distance.To do so, an equilibrium was found in which the sensor was kept close enough to ensure the entire jet was obtained, and far enough to avoid interference from the neighbor jets [25]. Also, the chamber pressure was controlled through valves connected to a pressurized nitrogen tank. Moreover, the holder is selected so that the sensor is aligned perpendicularly to the spray, as depicted in Figure 2.

2.2.2. Injection Rate Discharge Curve Indicator

Injection rate measurements were done with an injection rate discharge curve indicator (IRDCI), applying the Bosch long-tube methodology [28]. In Figure 3,

Published as: Applied Thermal Engineering, vol. 181, no. August, p. 115891, 2020. DOI: 10.1016/j.applthermaleng.2020.115891.

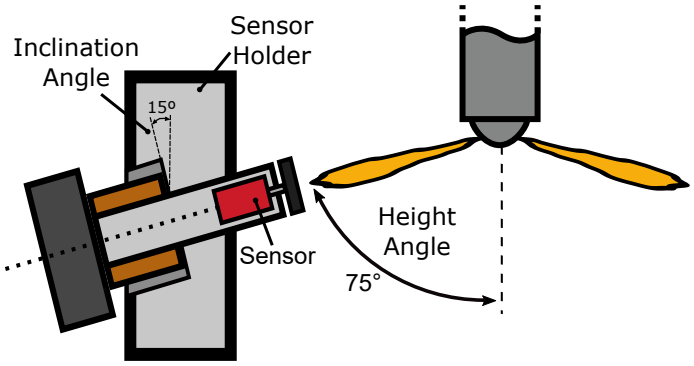

Figure 2: Sensor alignment in the momentum flux test rig.

a schematic diagram is illustrated. When fuel is injected into the measurement tube, a pressure wave is generated. The fast-response pressure sensor, a piezoelectric transducer, captures the pressure variation caused by the injection event. From the signal, it is possible to calculate the instantaneous mass flow rate, as explained by Salvador et al. [29].

Afterward, the wave travels at the speed of sound through the long tube that goes around the device, up to the release volume where it is dampened. Then, the fuel enters through a filter into the equalizing piston, which is pressurized on the other side by nitrogen set at the desired discharge pressure, sealing the outlet. Once the fuel-side sets the piston in equilibrium, any additional mass injected induces a pressure increase. In consequence, the piston moves, which unseals the exit, and lets a small amount of mass out of the IRDCI, equivalent to the mass injected. This mass is deposited into a downstream scale, and a mass flow rate measurement is obtained for comparison purposes [29]. The same refrigerating system detailed in the momentum flux section was employed to control the operating temperature of the injector.

2.3. Data Post-Processing

A high-speed acquisition system was utilized to record the signals provided by the sensors during the injection process, both for injection rate and momentum flux measurements. For multiple injections events, the main injection was

Published as: Applied Thermal Engineering, vol. 181, no. August, p. 115891, 2020. DOI: 10.1016/j.applthermaleng.2020.115891.

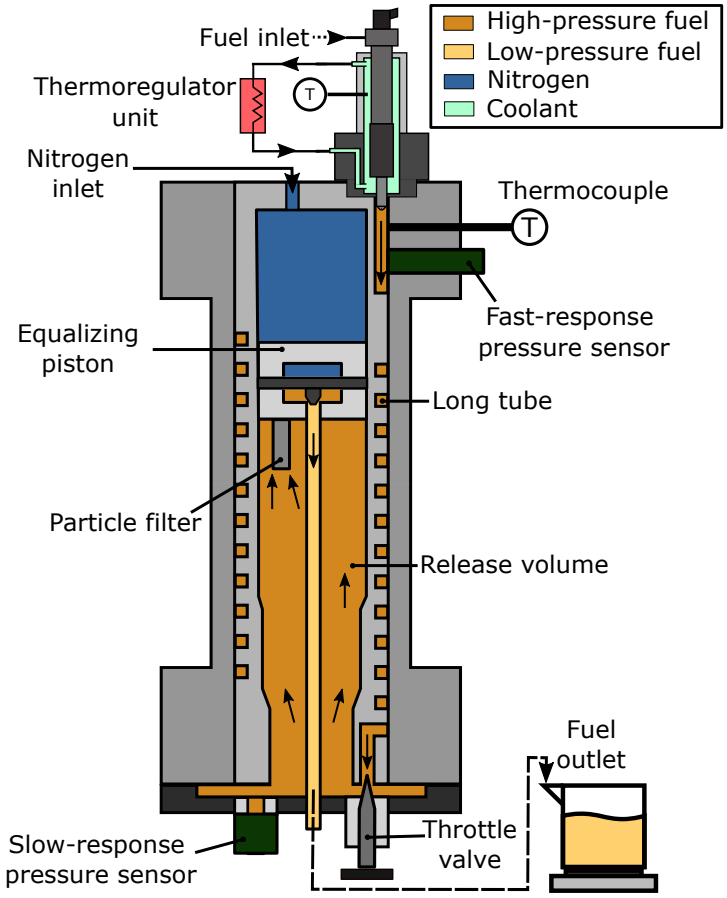

Figure 3: Injection Rate Discharge Curve Indicator schematic diagram.

decoupled from the pilot/post injection in order to measure the mass quantity injected in each event, as depicted in Figure 4. As the signal values were much higher than noise, it was possible to detect the start and end of each injection, calculating the rising and falling edge of each curve. Thus, the injection time limits were established, and the mass injected in each event was determined by integrating both curves between the limits, and the total mass by adding these values.

To eliminate measuring errors and uncertainties, 50 cycles of each test point were made and averaged into a final signal. Then, the signal is corrected to

account for the cumulative phenomenon [30]. Finally, shot-to-shot dispersion is evaluated through the relative standard deviation of the total injected mass, injection duration and stabilized injection rate, which was below 2% for every condition tested.

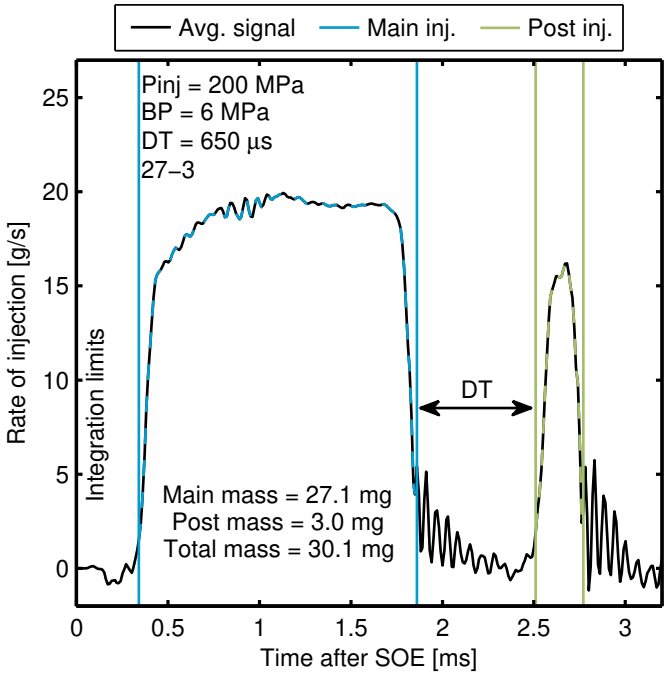

Figure 4: Decoupling of two injection pulses. The labeling 27-3 refers to the nominal strategy of 27 mg and 3 mg for the injected mass of main and post pulses respectively.

2.4. Test Matrix

Boundary conditions such as injection pressure, chamber density, and temperature, were selected using guidelines from the Engine Combustion Network (ECN) [31]. The amount of fuel per injection was elected using baseline points from a 1.6-liter engine, with an injected mass per cycle of 50 mg, equipped with 100 μm - 8-orifice injector. Quantities were scaled and rounded to the 90 μm - 6-orifice injector used, which resulted in an injected mass per cycle of 30 mg. Then, electrical pulses duration were adjusted for each multiple injec-

tion boundary condition to reach the targeted mass quantity of 30 mg between the pilot/post and main injection. These adjustments were established during the first campaign of measurements, and the same electrical signals were employed in the experiments done after aging, in order to compare the performance between each stage. Three fuel distribution schemes were analyzed: single, pilot-main, and main-post injection. For each multiple injection strategy, four different dwell times were tested.

Injection conditions employed throughout the experiments are depicted in Table 2 and Table 3. A reduced test matrix was employed to assess the status of the injector, in the momentum flux measurements. Commercially available diesel (EN590) was employed.

Table 2: Test plan for the momentum flux campaign.

Parameter	**Value**	**Units**
Injection pressure	100 - 200	MPa
Back pressure	5	MPa
Ambient gas	Nitrogen	-
Operating temperature (Injector)	363	K
Injection frequency	1	Hz
Cycles per test point	50	-

3. Results and discussions

The following section describes the results seen throughout the experiments. First, momentum flux measurements, taken to assess the status of the injector, are presented. Then, single injection measurements are detailed, which serve to observe more clearly the main differences before and after aging. Finally, the effects these phenomena have on multiple injection strategies are discussed.

Published as: Applied Thermal Engineering, vol. 181, no. August, p. 115891, 2020. DOI: 10.1016/j.applthermaleng.2020.115891.

Table 3: Test plan for the rate of injection campaign.

Parameter	Value	Units
Injection pressure	100 - 200	MPa
Back pressure	3 - 6	MPa
Operating temperature (Injector)	363	K
Pilot/post dwell times	200 - 350 - 500 - 650	μs
Pilot/post inj. quantity	1-3	mg
Main inj. quantity	29-27	mg
Total mass per multiple inj.	30	mg
Injection frequency	1	Hz
Cycles per test point	50	-

3.1. Momentum flux measurements

Figure 5 depicts momentum flux curves for each outlet hole of the injector at its new state (left plots) and after aging (right plots). All the holes have similar steady-state momentum flux values ($\dot{M}$) before aging, whereas holes 2 and 4 notably reduced their values after aging. Moreover, the geometrical diameters before aging of the orifices (provided by the manufacturer) are detailed in Table 4. All of them have similar values, being the maximum variation found between holes 2 and 3 with a 2.4 μm difference (representing a 2.6% variation only). Then, similar momentum flux curves were expected between orifices for the same boundary conditions, as seen on the subplots before aging of Figure 5. Thus, the considerable variations observed in the steady momentum flux after aging were not proportional to the differences between the diameters of the holes.

Moreover, Table 4 contains momentum coefficient (C_M) values after aging, which were calculated by the Equation 1 [25]:

$$C_M = \frac{\dot{M}}{\dot{M}_{theor}} = \frac{\dot{M}}{2A_o\Delta P} \tag{1}$$

Where A_o represents the theoretical outlet area of the orifice and ΔP the

Published as: Applied Thermal Engineering, vol. 181, no. August, p. 115891, 2020. DOI: 10.1016/j.applthermaleng.2020.115891.

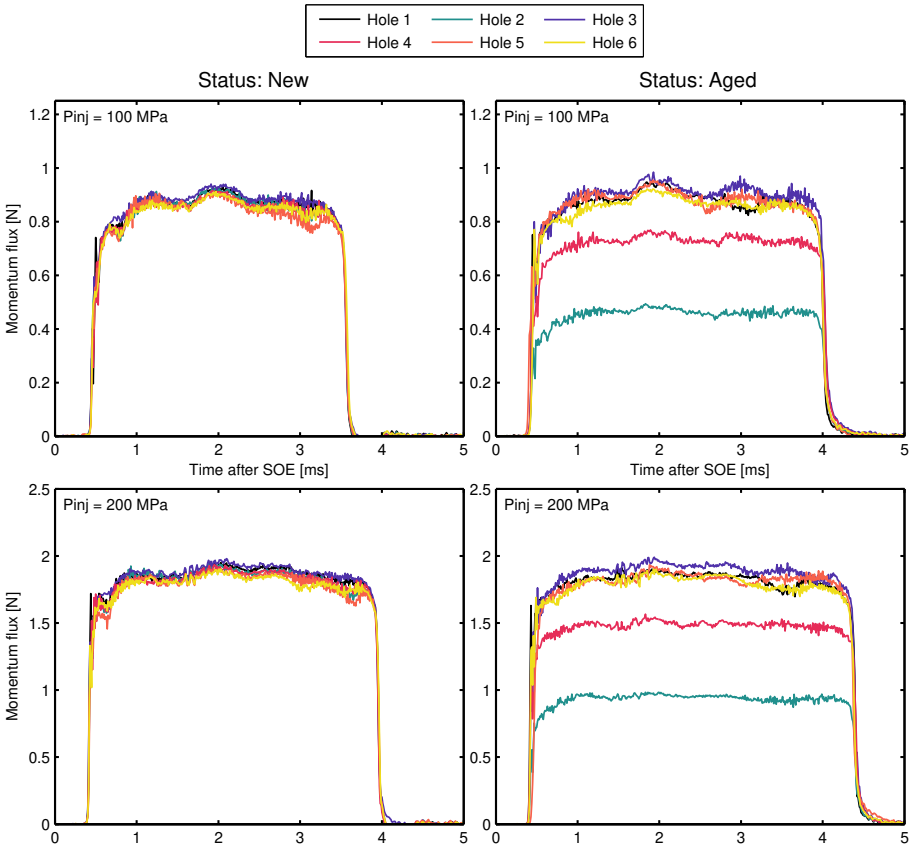

Figure 5: Momentum flux measurement for each hole of the injector before and after aging. BP: 5 MPa, ET: 1.5 ms.

difference between the injection pressure and the back pressure. This coefficient compares the experimental steady momentum flux with the theoretical value, which considers the total availability of the orifice area. Moreover, this coefficient is directly correlated to the area coefficient ($C_M \propto C_a$) [25], which evaluates the effective area (A_{eff}) being employed, in comparison to the total theoretical area available [25]:

$$C_a = \frac{A_{eff}}{A_o} \tag{2}$$

Thus, the momentum coefficient serves as a qualitative measurement of the

Published as: Applied Thermal Engineering, vol. 181, no. August, p. 115891, 2020. DOI: 10.1016/j.applthermaleng.2020.115891.

Table 4: Piezoelectric injector diameters before aging and momentum coefficient after aging.

Hole	**Diameter [μm]**	$\mathbf{C_M}$
1	90,1	0,74
2	89,3	**0,39**
3	91,7	0,74
4	89,7	**0,60**
5	89,6	0,75
6	89,9	0,73
Average	90,3	0,74

amount of area being used in each orifice. As holes 1, 3, 5, and 6 had similar results before and after aging, their values were averaged and served as reference values (last row of Table 4). Regarding the momentum coefficient, hole 2 had a value of 0.39, which represented 47% less than the reference value (0.74). Furthermore, hole 4 (0.60) saw its value reduced by 19%, when compared to the reference value. Then, a considerable decrease in momentum coefficient values was perceived in holes 2 and 4.

These variations in momentum flux curves were attributed to the presence of deposits in those holes. In this sense, the existence of deposits would reduce the available area and obstruct the path of the fuel throughout the orifice, reducing the effective outlet flow.

3.2. Rate of injection measurements

3.2.1. Single injection

Figure 6 depicts the rate of injection at two stages of the lifetime of the injector: at its new and at its aged state. It can be seen that, for the same boundary conditions, the injector had a longer injection duration once it aged. Specifically, the injection started at the same moment, but the injector took a longer time to end the injection after aging. Furthermore, the injector developed a lower steady-state injection rate flow as well.

The extended duration phenomenon led to an increase in the injected mass, whereas the lower steady injection rate caused its reduction. For each injection event, the predominant phenomenon depended on the boundary conditions, which could lead to higher or lower injected mass after aging. For instance, in Figure 6, the lower injection rate had a predominant effect, leading to a 6.2% decrease of the injected mass after aging. These phenomena were continuously observed throughout the measurements campaign and will be discussed in detail in the following sections.

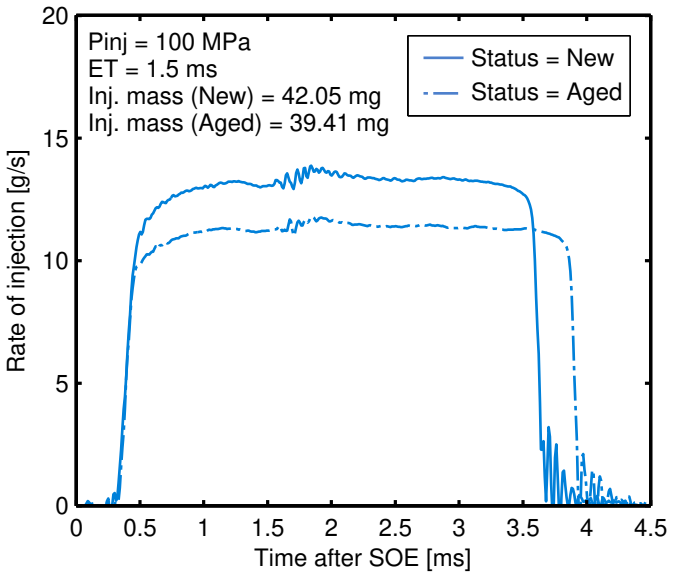

Figure 6: Rate of injection measurement before and after aging.

The reduction in steady flow after aging is also reflected in the discharge coefficient (C_d) [32] values depicted in Figure 7. For every condition tested, a decrease of the coefficient value after aging can be observed due to losses in the efficiency of the flow delivery of the injector. For each status, the averaged discharge coefficient value was calculated as the mean of the coefficients obtained from every boundary condition measured. The discharge coefficient of each test

point was calculated by the Equation 3 [24]:

$$C_d = \frac{\dot{m}}{\dot{m}_{theor}} = \frac{\dot{m}}{2A_o\rho_f\Delta P} \tag{3}$$

In which ρ_f represents the density of the fuel for each test condition.

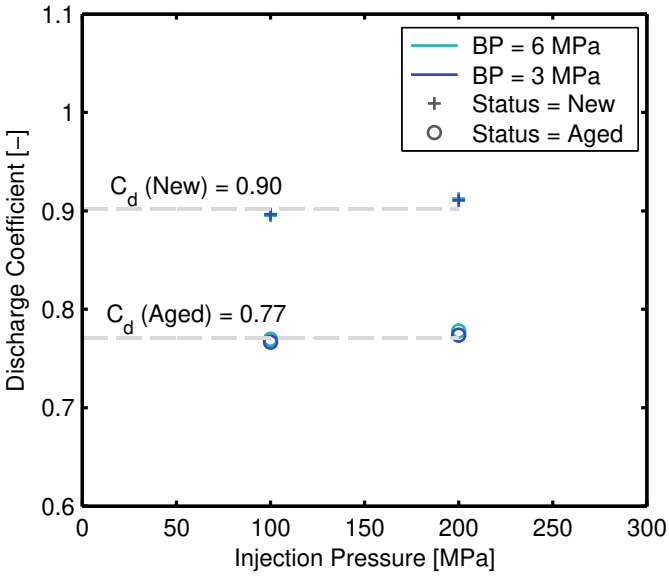

Figure 7: Discharge coefficient values for each status.

.

The partial obstruction of the nozzle orifices (evaluated in the previous section) was pointed out as a possible explanation of the variations observed after aging. Specifically, the appearance of deposits would reduce the effective outlet area of the fuel, restricting the flow exiting through the outlet holes. As a consequence, the effective steady-state injection rate would decrease, as seen in Figure 6.

Furthermore, the existence of fouling could also explain the difference seen in the injection duration. In this sense, obstructions would not affect the start of injection given that, due to the needle dynamics, the injector is less sensible to the presence of fouling in the nozzle, and more to the control volume status [33]. Specifically, if the control volume performs correctly, the upwards needle

movement would be unaltered, diesel fuel would flow to the nozzle at the same rate after start of energizing and start of injection should not be affected, as depicted in Figure 6. On the other hand, the outlet holes state could affect the end of injection (EOI) after the end of energizing (EOE), as a nozzle with obstructed holes would have a lower discharge coefficient [25], as observed in Figure 7. Consequently, the fuel would take a longer time evacuating the sac, increasing the sac pressure throughout the descend of the needle. As the force pushing the needle downwards remains constant in value, the needle will require a longer time to complete its path, seal the outlet holes, and end the injection.

Additionally, the appearance of deposits in the control volume holes was considered as another possible cause of the variations seen in the injection duration after aging, as changes in the effective area of the inlet or outlet orifice of the control volume have an important effect in the injection process [33]. Specifically, the presence of deposits in the inlet orifice would decrease its effective diameter, restricting the combustible flowing into the control volume. Thus, a longer time would be required to fill the volume and regain the pressure needed to push the needle downwards, extending the EOI, as depicted in Figure 6.

3.2.2. Pilot-main injections

In Figure 8, a pilot-main injection is depicted for the new and aged status of the injector, employing the same electrical signal and boundary conditions between statuses. It can be seen that the steady-state injection rate value is lower after aging, which is attributed to the obstructed holes in the nozzle, as explained in the previous section. Furthermore, each injection started at the same time for both statuses but took a longer time to end after aging. This difference was particularly noticeable in the main injection, which was longer and steadier than the pilot injection.

This trend was observed through all the pilot-main conditions analyzed and could be related to the events occurring inside the injector: when the piezo-stack is energized for a small period (pilot/post injection), a transient behavior is predominant, as the injection does not or barely reaches a steady-state flow

Published as: Applied Thermal Engineering, vol. 181, no. August, p. 115891, 2020. DOI: 10.1016/j.applthermaleng.2020.115891.

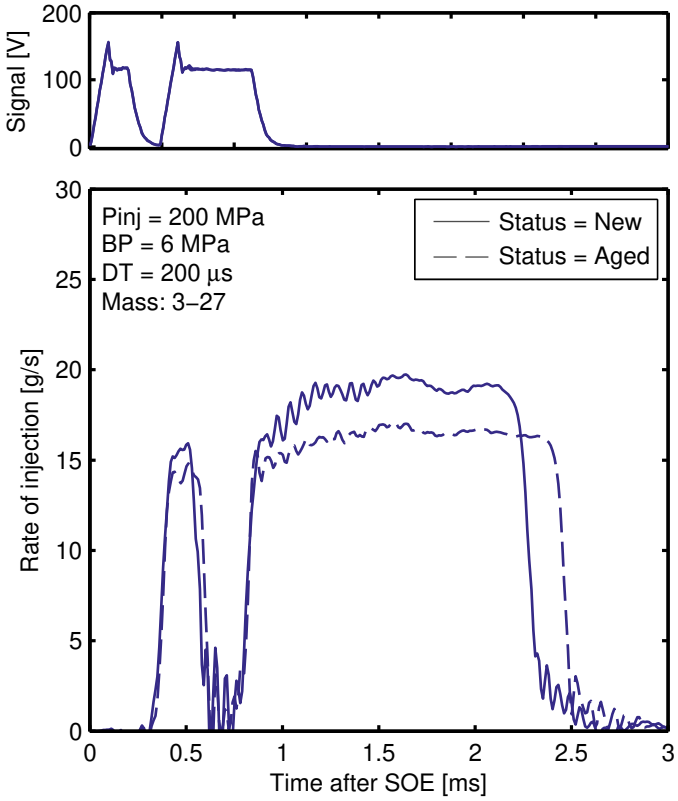

Figure 8: Pilot injection strategy for both statuses.

status. Thus, there is not enough time for the needle to complete its upwards movement and establish a steady flow, as the control volume is quickly re-filled and pressurized, stopping the needle. Then, the end of injection would be faster: as the needle is closer to the sac and the pressure difference between the control volume and the sac did not fully develop, the shorter route downwards to seal the sac is completed rapidly. Thus, the effects produced by the presence of deposits in the outlet holes are diminished. However, if the ET is long enough for a steady injection flow to establish (as in the main injection), the effects of deposits appearance in the nozzle become predominant. A broader view of these events is depicted in Figure 9. It is observed that the pilot injection was not greatly affected by the injector status after aging.

Published as: Applied Thermal Engineering, vol. 181, no. August, p. 115891, 2020. DOI: 10.1016/j.applthermaleng.2020.115891.

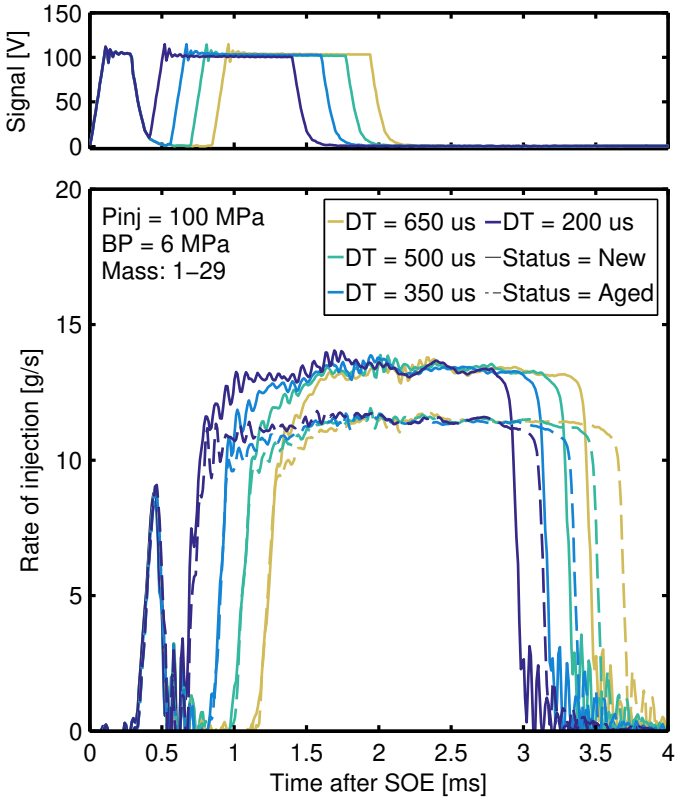

Figure 9: Pilot injection for multiple hydraulic dwell times.

Furthermore, Figure 10 shows the percentage variation of the injected mass in comparison with the targeted mass of 30 mg, for every pilot-main condition tested. As previously noted, the target was to inject 30 mg in each multiple injection event, in 1-29 or 3-27 proportions. The electrical signal required to reach this goal was determined during the new status measurements and employed after aging as well, to study these variations. The percentage variation for every DT is shown before and after aging. Additionally, the numeric mass variation value after aging is written in each subplot.

As the signals were conditioned during the new status, the injections made at this stage had no variation regarding the targeted mass. On the other hand, pilot-main injections made after aging suffered some variations, generally lower

Published as: Applied Thermal Engineering, vol. 181, no. August, p. 115891, 2020. DOI: 10.1016/j.applthermaleng.2020.115891.

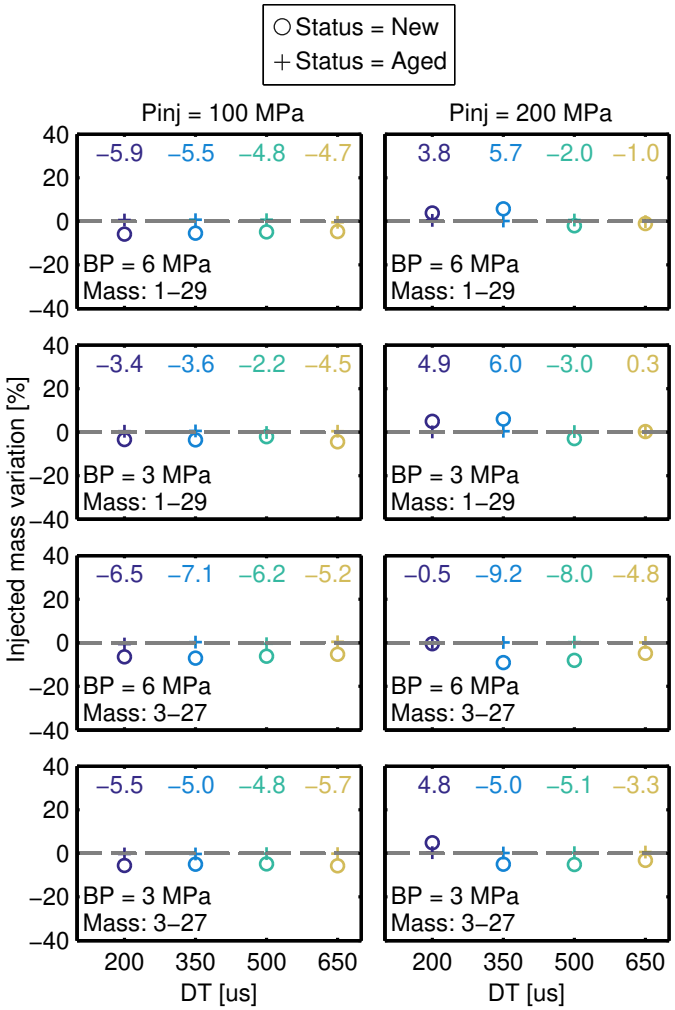

Figure 10: Percentage variation of the injected mass, regarding the targeted mass of 30 mg.

than 6%. In this sense, the lower steady injection rate results in a reduction of the injected mass, whereas the extended injection duration increases it. Thus, a balance is made in which an effect will be more or less predominant, depending on the boundary conditions. For instance, an increase of the injection pressure would extend the closing HD [34], increasing the injected mass quantity, as seen in Figure 10. It can also be observed that the same effect is produced by reducing the back pressure.

3.2.3. Main-post injections

In Figure 11, a main-post injection event for both statuses of the injector is shown, maintaining the boundary conditions. It can be seen that, for the same electrical pulse, the aged injector is not able to separate the main and post injection, resulting in a unique and large injection.

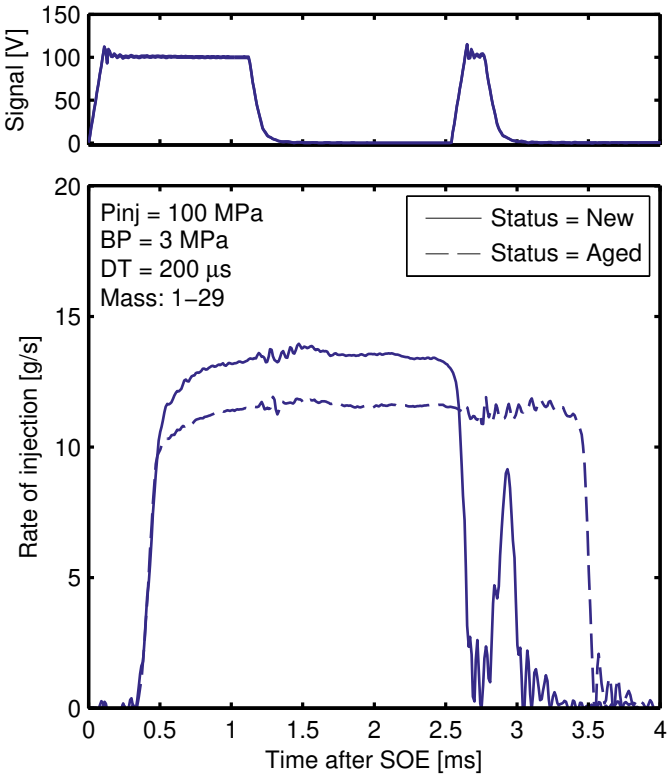

Figure 11: Post injection strategy for both statuses.

This behavior was continually seen for every main-post injection after aging with a dwell time of 200 μs, as seen, for instance, in Figure 12. Curves with 650μs and 300μs of dwell time have been omitted, allowing more viewing clarity on the post injection zone without losing insights on the phenomena observed.

As previously discussed, the variations in behavior after aging mainly affects the duration of the larger and steadier injections. Thus, the pilot (short and

Published as: Applied Thermal Engineering, vol. 181, no. August, p. 115891, 2020. DOI: 10.1016/j.applthermaleng.2020.115891.

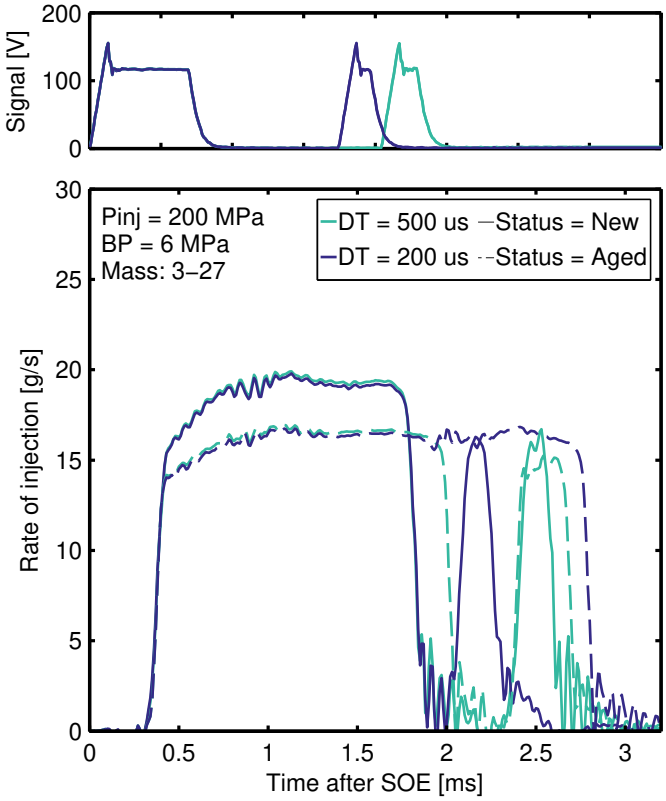

Figure 12: Post injection strategy for multiple hydraulic dwell times.

transient) injection did not affect the start of the following main injection, as depicted in Figure 9. However, in post injection strategies the extended duration of the preceding main injection could have a considerable impact on the post injection event: if the dwell time between the main and post injection is short enough, the extended time required by the injector after aging to end the injection could overlap with the start of the post injection. In other words, the electrical pulse of the post injection could be sent before the needle develops its downwards movement to end the main injection, resulting in a unique injection with a larger closing HD.

Furthermore, the union of the main and post injections affects the quantity of fuel injected. Specifically, fuel was continuously injected from the start of the

Published as: Applied Thermal Engineering, vol. 181, no. August, p. 115891, 2020. DOI: 10.1016/j.applthermaleng.2020.115891.

main to the end of the post injection, rather than stopping between injections. Thus, not only the benefits of the post injection are lost, but an increase in fuel consumption would appear. Figure 13 summarizes the percentage variation of the injected mass for every condition studied, in comparison with the targeted mass of 30 mg.

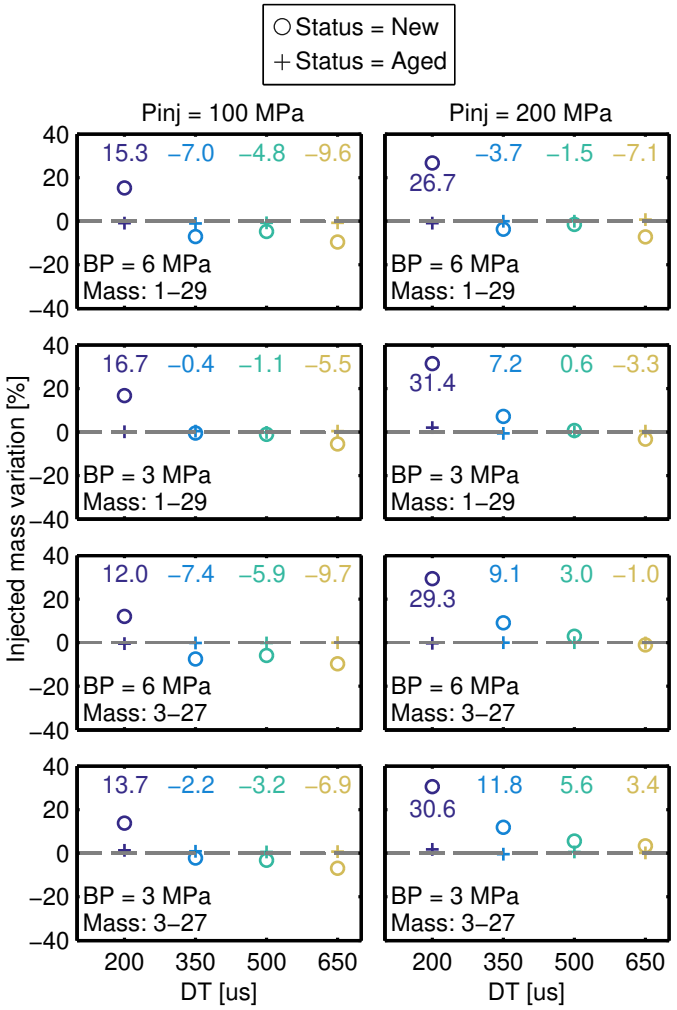

Figure 13: Percentage variation of the injected mass, in comparison with the targeted mass of 30 mg.

It can be seen that the mass variation is generally higher for post injection

strategies, as they are more sensitive to increased main injection duration. Furthermore, it is depicted that the union of main and post injection produces a considerable increase in the total injected mass, as seen for the DT of 200 μs. This effect is intensified with larger injection pressures, as this increase also extends the closing HD [34].

4. Summary and conclusions

This study analyzes the influence of aging of a diesel injector on multiple injection strategies. To do so, injection rate measurements were done at two stages of the injector's lifetime: once when it was brand new, and another one after aging, following 1400 hours of use with an injection frequency of 0.25 Hz within a test rig capable of emulating real engine conditions of temperature and pressure. From the obtained results, the following main conclusions are drawn:

- The status of the injector was assessed with momentum flux measurements, which confirmed the partial obstruction of two outlet orifices of the nozzle.
- Injection rate measurements showed that, for the same electric pulse, the steady-state rate of injection was lower and longer after aging, affecting the total fuel mass injected.
- The extension of the injection duration after aging was more significant when the injection was longer and reached a stabilized state.
- The partial obstruction of the nozzle orifices was pointed out as a possible explanation of the variations observed in the injection rate after aging.
- The extended duration of the main injection could overlap with the start of the post injection, resulting in a single injection. Hence, not only an increase in fuel consumption would appear, but the thermal benefits of implementing the post injection would be lost.

References

[1] T. Johnson, Vehicular Emissions in Review, SAE International Journal of Engines 9 (2016) 1258–1275. doi:10.4271/2016-01-0919.

[2] S. Mendez, B. Thirouard, Using Multiple Injection Strategies in Diesel Combustion: Potential to Improve Emissions, Noise and Fuel Economy Trade-Off in Low CR Engines, SAE Technical Paper 2008-01-1329 1 (2008) 662–674. doi:10.4271/2008-01-1329.

[3] S. D'Ambrosio, A. Ferrari, Potential of double pilot injection strategies optimized with the design of experiments procedure to improve diesel engine emissions and performance, Applied Energy 155 (2015) 918–932. doi:10.1016/j.apenergy.2015.06.050.

[4] P. Carlucci, A. Ficarella, D. Laforgia, Effects on combustion and emissions of early and pilot fuel injections in diesel engines, International Journal of Engine Research 6 (2005) 43–60. doi:10.1243/146808705X7301.

[5] P. Carlucci, A. Ficarella, D. Laforgia, Effects of pilot injection parameters on combustion for common rail diesel engines, SAE Technical Paper 2003-01-0700 (2003). doi:10.4271/2003-01-0700.

[6] J. M. Desantes, J. M. García-Oliver, A. García, T. Xuan, Optical study on characteristics of non-reacting and reacting diesel spray with different strategies of split injection, International Journal of Engine Research (2018). doi:10.1177/1468087418773012.

[7] J. Benajes, J. Martín, A. García, D. Villalta, A. Warey, Swirl ratio and post injection strategies to improve late cycle diffusion combustion in a light-duty diesel engine, Applied Thermal Engineering 123 (2017) 365–376. doi:10.1016/j.applthermaleng.2017.05.101.

[8] J. O'Connor, M. P. B. Musculus, L. M. Pickett, Effect of post injections on mixture preparation and unburned hydrocarbon emissions in a heavy-duty

diesel engine, Combustion and Flame 170 (2016) 111–123. doi:10.1016/j.combustflame.2016.03.031.

[9] M. Bobba, M. P. B. Musculus, W. Neel, Effect of Post Injections on In-Cylinder and Exhaust Soot for Low-Temperature Combustion in a Heavy-Duty Diesel Engine, SAE International Journal of Engines 3 (2010) 2010–01–0612. doi:10.4271/2010-01-0612.

[10] E. Mancaruso, S. S. Merola, B. M. Vaglieco, Study of the multi-injection combustion process in a transparent direct injection common rail diesel engine by means of optical techniques, International Journal of Engine Research 9 (2008) 483–498. doi:10.1243/14680874JER01308.

[11] Z. Zheng, L. Yue, H. Liu, Y. Zhu, X. Zhong, M. Yao, Effect of two-stage injection on combustion and emissions under high EGR rate on a diesel engine by fueling blends of diesel/gasoline, diesel/n-butanol, diesel/gasoline/n-butanol and pure diesel, Energy Conversion and Management 90 (2015) 1–11. doi:10.1016/j.enconman.2014.11.011.

[12] S. Yoon, H. Kim, D. Kim, S. Park, Effect of Fuel Injection Strategy on DPF Regeneration in Single Cylinder Diesel Engine, in: ASME Internal Combustion Engine Division Fall Technical Conference, Houston, 2015. doi:10.1115/icef2015-1140.

[13] H. Liu, B. Mao, J. Liu, Z. Zheng, M. Yao, Pilot injection strategy management of gasoline compression ignition (GCI) combustion in a multi-cylinder diesel engine, Fuel 221 (2018) 116–127. doi:10.1016/j.fuel.2018.01.073.

[14] O. Hofmann, P. Strauß, S. Schuckert, B. Huber, D. Rixen, G. Wachtmeister, Identification of Aging Effects in Common Rail Diesel Injectors Using Geometric Classifiers and Neural Networks, SAE Technical Papers 2016-April (2016). doi:10.4271/2016-01-0813.

[15] A. T. Hoang, A. T. Le, A review on deposit formation in the injector of diesel engines running on biodiesel, Energy Sources, Part A: Recovery,

Utilization and Environmental Effects 41 (2019) 584–599. doi:10.1080/15567036.2018.1520342.

[16] D. E. Winterbone, E. Clough, K. K. Rao, P. Richards, D. Williams, The effect of di nozzle fouling on fuel spray characteristics, SAE Technical Papers (1992). doi:10.4271/922232.

[17] P. Richards, R. D. Walker, D. Williams, Fouling of two stage injectors - An investigation into some causes and effects, SAE Technical Papers (1997). doi:10.4271/971619.

[18] R. Caprotti, N. Bhatti, I. Nobuyuki, Protecting diesel fuel injection systems, SAE Technical Papers (2011). doi:10.4271/2011-01-1927.

[19] A. M. Liaquat, H. H. Masjuki, M. A. Kalam, I. M. Rizwanul Fattah, Impact of biodiesel blend on injector deposit formation, Energy 72 (2014) 813–823. doi:10.1016/j.energy.2014.06.006.

[20] J. Ullmann, M. Geduldig, H. Stutzenberger, R. Caprotti, G. Balfour, Investigation into the Formation and Prevention of Internal Diesel Injector Deposits, SAE Technical Paper 2008-01-0926 (2008) —-. doi:10.4271/2008-01-0926.

[21] W. Urzędowska, Z. Stępień, Prediction of threats caused by high FAME diesel fuel blend stability for engine injector operation, Fuel Processing Technology 142 (2016) 403–410. doi:10.1016/j.fuproc.2015.11.001.

[22] R. Payri, J. Gimeno, S. Cardona, S. Ayyapureddi, Experimental study of the influence of the fuel and boundary conditions over the soot formation in multi-hole diesel injectors using high-speed color diffused back-illumination technique, Applied Thermal Engineering 158 (2019) 113746. doi:10.1016/J.APPLTHERMALENG.2019.113746.

[23] D. Schöppe, C. Stahl, G. Krüger, V. Dian, Servo-Driven Piezo Common Rail Diesel Injection System, MTZ worldwide 73 (2012) 18–23. doi:10.1365/s35595-012-0107-y.

[24] R. Payri, G. Hardy, J. Gimeno, A. Bautista, Analysis of counterbore effect in five diesel common rail injectors, Experimental Thermal and Fluid Science 107 (2019) 69–78. doi:10.1016/j.expthermflusci.2019.05.008.

[25] R. Payri, J. M. Garcia-Oliver, F. J. Salvador, J. Gimeno, Using spray momentum flux measurements to understand the influence of diesel nozzle geometry on spray characteristics, Fuel 84 (2005) 551–561. doi:10.1016/j.fuel.2004.10.009.

[26] S. Som, A. I. Ramirez, D. E. Longman, S. K. Aggarwal, Effect of nozzle orifice geometry on spray, combustion, and emission characteristics under diesel engine conditions, Fuel 90 (2011) 1267–1276. doi:10.1016/j.fuel.2010.10.048.

[27] R. Payri, J. Gimeno, C. Mata, A. Viera, Rate of injection measurements of a direct-acting piezoelectric injector for different operating temperatures, Energy Conversion and Management 154 (2018) 387–393. doi:10.1016/j.enconman.2017.11.029.

[28] W. Bosch, The Fuel Rate Indicator: A New Measuring Instrument for Display of the Characteristics of Individual Injection, SAE Technical Paper 660749 (1966). doi:10.4271/660749.

[29] F. J. Salvador, J. Gimeno, M. Carreres, M. Crialesi-Esposito, Fuel temperature influence on the performance of a last generation common-rail diesel ballistic injector. Part I: Experimental mass flow rate measurements and discussion, Energy Conversion and Management 114 (2016) 364–375. doi:10.1016/j.enconman.2016.02.042.

[30] R. Payri, F. J. Salvador, J. Gimeno, G. Bracho, A new methodology for correcting the signal cumulative phenomenon on injection rate measurements, Experimental Techniques 32 (2008) 46–49. doi:10.1111/j.1747-1567.2007.00188.x.

[31] ECN, Engine Combustion Network, Online, 2010. URL: www.sandia.gov/ecn/.

[32] S. Essien, A. Archibong-Eso, L. Lao, Discharge coefficient of high viscosity liquids through nozzles, Experimental Thermal and Fluid Science 103 (2019) 1–8. doi:10.1016/j.expthermflusci.2019.01.004.

[33] F. J. Salvador, M. Carreres, M. Crialesi-Esposito, A. H. Plazas, Determination of critical operating and geometrical parameters in diesel injectors through one dimensional modelling, design of experiments and an analysis of variance, Proceedings of the Institution of Mechanical Engineers, Part D: Journal of Automobile Engineering 232 (2018) 1762–1781. doi:10.1177/0954407017735262.

[34] E. Plamondon, P. Seers, Development of a simplified dynamic model for a piezoelectric injector using multiple injection strategies with biodiesel/diesel-fuel blends, Applied Energy 131 (2014) 411–424. doi:10.1016/j.apenergy.2014.06.039.

Acknowledgments

This work has been partially funded by Spanish Ministerio de Ciencia, Innovación y Universidades through project RTI2018-099706-B-100.

Tomas Montiel was supported by a research grant from Generalitat Valenciana and the European Union (Reference: ACIF/2018/122).